

INTERACTION BETWEEN GASES AND LIQUIDS IN HOLLOW, COMPOUND JETS AT LOW REYNOLDS NUMBERS

J. I. Ramos

Room I-325D, E.T.S. Ingenieros Industriales, Universidad de Málaga
Plaza El Ejido, s/n, 29013-Málaga, Spain

Although there has been quite a lot research on the development of one-dimensional, mathematical models for the analysis of single-component filaments and jets under both isothermal and non-isothermal conditions at low Reynolds numbers, hollow, compound fibers (Figure 1) such as those used in reinforced materials and modern optical fibers (which are manufactured in coextrusion processes) have received very little attention despite the fact that the combination of two or more different materials with different properties may result in hollow, composite fibers which highly desirable properties. For example, in the manufacture of traditional optical fibers, the core is surrounded by a sheath of cladding material, whereas hollow, compound fibers that enclose an air ring may be used as almost ideal tunable filters. These fibers are usually manufactured by means of fiber spinning processes which consist of the steady extrusion of hot melts through a series of small holes in a plate (spinnerets) into ambient air; the resulting extrudates are simultaneously extended and wound up on a rapidly rotating drum (godet). Freezing takes place between the spinneret and the godet, and, usually, large extensions rates, rapid cooling, and high speeds are involved.

One of the main issues in the manufacture of hollow, compound fibers is the stability of the spinning process and, in particular, a nonlinear phenomenon that is called draw resonance. The objective of this paper is several-fold. First, an asymptotic analysis of axisymmetric, hollow, compound, isothermal, Newtonian jets of large aspect ratio at low Reynolds numbers is performed by means of perturbation techniques based on the smallness of the aspect ratio. Second, the leading-order equations of the asymptotic analysis are solved numerically to determine the effects of the compression and expansion of the gases enclosed by the inner, annular jet on the time-dependent fluid dynamics of hollow, compound jets when subjected to time-dependent velocities at the upstream and/or downstream boundaries.

The inner and outer annular jets correspond to $R_1(t, x) \leq r \leq R(t, x)$ and $R(t, x) \leq r \leq R_2(t, x)$ with $R_1(t, x) \neq 0$. The fluid dynamics of isothermal, axisymmetric, hollow, compound jets are

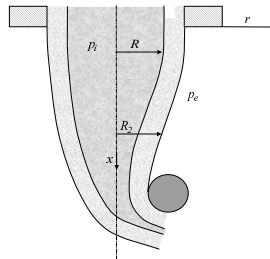


Figure 1: Schematic of a hollow, compound, annular liquid jet.

governed by the conservation equations of mass and linear momentum, and kinematic and dynamic boundary conditions at the jet's interfaces, $R_1(t, x)$, $R(t, x)$ and $R_2(t, x)$, where R corresponds to the interface between the inner and outer annular jets, t is time and x and r are the axial and radial coordinates, respectively. The kinematic conditions establish that the hollow, compound jet's interfaces are material surfaces where the shear stress is continuous, and the jump in normal stresses across the interfaces is balanced by surface tension. Since there are three interfaces, there are three surface tensions, i.e., $\sigma_i, i = 1, 2$, is the surface tension at the inner jet's inner surface and at the outer jet's outer surface, respectively, and σ is the surface tension at the interface between the inner and outer, annular jets. The gases that surround the outer jet and those enclosed by the inner one have been assumed to be dynamically passive since, in general, they have smaller density and dynamic viscosity than those of liquids, and their pressures are denoted by $p_e(t)$ and $p_i(t)$, respectively. This implies that the gases surrounding the liquid may not introduce strong velocity variations on each cross section of the jet, although they may affect its dynamics. Moreover, for viscous fluids, $(\mathbf{v}_2 - \mathbf{v}_1) \cdot \mathbf{n} = (\mathbf{v}_2 - \mathbf{v}_1) \cdot \mathbf{t} = 0$ where \mathbf{n} and \mathbf{t} denote the unit vectors normal and tangent, respectively, to $r = R(t, x)$, \mathbf{v} denotes the velocity vector, and the subscripts 1 and 2 refer to the inner and outer, respectively, annular jets. In this paper, a long wavelength approximation is used to reduce the time-dependent, two-dimensional governing equations to a more manageable (and easier to solve) one-dimensional set of equations by means of asymptotic methods based on the slenderness ratio, at low Reynolds numbers. These methods are based on the nondimensionalization of the radial and axial coordinates, time, axial and radial velocity components, and pressure, i.e., r, x, t, u, v and p , respectively, with respect to $R_0, \lambda, \lambda/u_0, u_0, v_0$ and $\mu u_0/\lambda$, respectively, where R_0 and λ denote a characteristic radius and a characteristic wave length in the axial direction, respectively, u_0 is a characteristic (constant) axial velocity component, $v_0 = R_0 u_0/\lambda$, and μ is a reference dynamic viscosity which here is taken as μ_2 . Substitution of these nondimensional variables into the governing equations and boundary conditions results in a system of equations which contain $\epsilon = R_0/\lambda$, $Re_2 = \rho_2 u_0 R_0/\mu_2$, $Fr = u_0^2/gR_0$, $Ca_2 = \mu_2 u_0/\sigma_2$, i.e., the slenderness ratio, and the Reynolds, Froude and capillary numbers, respectively, where g and ρ denote the gravitational acceleration and the liquid's density.

For small Reynolds numbers, $Re_2 = \epsilon Re$ with $Re = O(1)$, and, depending on the magnitude of the Froude and capillary numbers, several flow regimes can be identified. Here, we consider $Fr = F/\epsilon$ and $Ca_2 = Ca/\epsilon$ which correspond to low gravitational fields and small surface tension. Substitution of these values and expansion of the dependent variables as

$$\phi = \phi_0 + \epsilon^2 \phi_2 + O(\epsilon^4), \quad (1)$$

where ϕ denotes dependent variables, i.e., $u, v, p, R_i, i = 1, 2$, and R , in the governing equations and boundary conditions, together with the expansion of the boundary conditions around $R_0(t, x)$, $R_{10}(t, x)$ and $R_{20}(t, x)$ yield asymptotic expansions which at leading order, i.e., at $O(\epsilon^0)$, can be written as

$$u_{i0} = B_i(t, x), \quad p_{i0} = D_i(t, x), \quad v_{i0} = C_i(t, x)/r - B_{ix}r/2, \quad i = 1, 2, \quad (2)$$

$$B_1 = B_2, \quad p_{20} = D_2 = p_e + 1/(CaR_{20}) - 2(C_2/R_{20}^2 + B_{2x}/2), \quad (3)$$

$$p_{10} = D_1 = p_i - \sigma_1/(\sigma_2 Ca R_{10}) - 2(\mu_1 \mu_2)(C_1/R_{10}^2 + B_{1x}/2), \quad (4)$$

$$C_1 = \frac{p_i - p_e - 1/Ca \left(\frac{\sigma}{\sigma_2} \frac{1}{R_0} + \frac{\sigma_1}{\sigma_2} \frac{1}{R_{10}} + \frac{1}{R_{20}} \right)}{2 \left(\frac{1}{R_0^2} - \frac{1}{R_{20}^2} + \frac{\mu_1}{\mu_2} \left(\frac{1}{R_{10}^2} - \frac{1}{R_0^2} \right) \right)}, \quad (5)$$

$$(A_2)_t + (B_1 A_2)_x = 0, \quad (A_1)_t + (B_1 A_1)_x = 0, \quad 2C_1 = 2C_2 = (R_0^2)_t + (B_1 R_0^2)_x, \quad (6)$$

where $A_1 = (R_0^2 - R_{10}^2)/2$ and $A_2 = (R_{20}^2 - R_0^2)/2$.

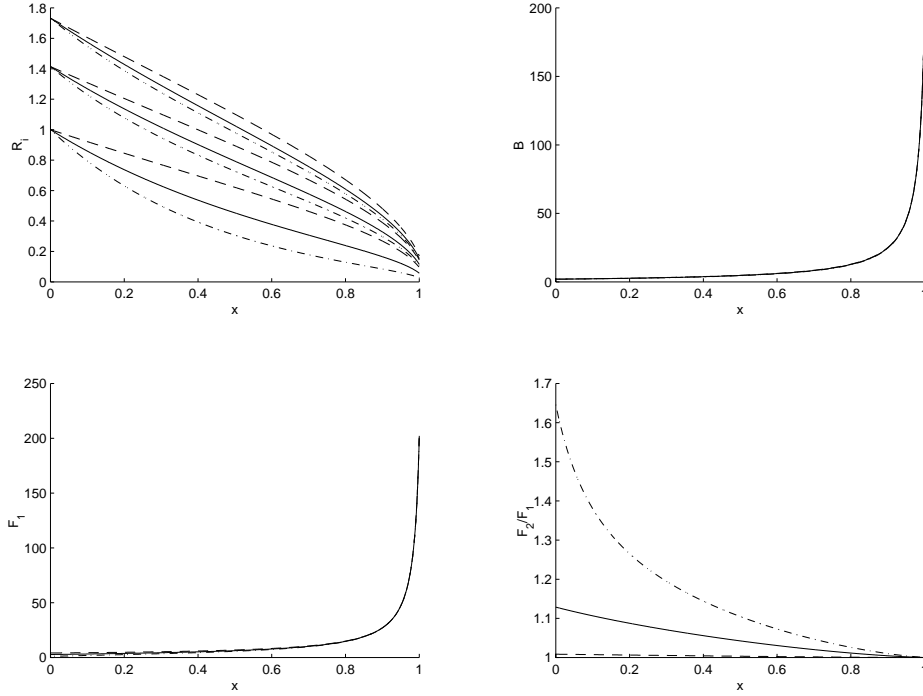


Figure 2: Hollow, compound jet's geometry (top left), axial velocity (top right), axial traction in the inner liquid (bottom left) and ratio of axial traction in the outer liquid to that in the inner one (bottom right) as function of the axial coordinate. ($Re = Re/Fr = \rho_1/\rho_2 = \mu_1/\mu_2 = \sigma/\sigma_2 = \sigma_1/\sigma_2 = \dot{v}_1 = \dot{v}_2 = 1$, $p_i = p_e = 0$; $Ca = 1$: solid lines; $Ca = 10$: dashed lines; $Ca = 0.5$: dashed-dotted lines).

The above equations contain seven unknowns, and, therefore, they are not a closed system. In order to close this system of equations, we first determine the $O(\epsilon^2)$ approximations of the axial momentum equation and shear stresses conditions at the three interfaces of the hollow, compound jet, which yield the following expression

$$\begin{aligned}
 Re (A_2 + \rho_1 A_1/\rho_2) ((B_1)_t + B_1(B_1)_x) &= Re/F (A_2 + \rho_1 A_1/\rho_2) + 3 ((A_2 + \mu_1 A_1/\mu_2) (B_1)_x) \\
 &+ (1/Ca) (A_2/R_{20}^2 (R_{20})_x - (\sigma_1/\sigma_2)(A_1/R_{10}^2)(R_{10})_x) + (2A_2/R_{20}^2 + 2\mu_1/\mu_2 A_1/R_{10}^2) C_x \\
 &+ 2C_1 ((\mu_1/\mu_2 - 1) (R_0)_x/R_0 - R_0^2 (\mu_1/\mu_2 (R_{10})_x/R_{10}^3 - (R_{20})_x/R_{20}^3)). \quad (7)
 \end{aligned}$$

Equations (5)-(7) clearly show the coupling between the pressure of the gases enclosed by the hollow, compound jet and the dynamics of the liquids that constitute the hollow, compound jet. For steady flows, Eq. (6) can be easily integrated but the solution of Eq. (7) requires numerical techniques. For time-dependent phenomena associated with inlet or take-up velocity fluctuations or variations of the pressure of the gases enclosed by the hollow, compound jet, Eqs. (5)-(7) are nonlinear and of the mixed hyperbolic-parabolic type. Equation (7) was solved by means of implicit, second-order accurate in both space and time finite difference method, whereas Eq. (6) was discretized by means of upwind differences in space and second-order accurate finite difference in time, and the resulting system of nonlinear algebraic equations was solved iteratively until the differences between two successive values was less than 10^{-12} . The minimum number of grid points used in the x -direction was 2002, and the time step was selected so that the calculations were independent of this step.

Some sample results illustrating the effects of the capillary number and pressure of the gases enclosed by steady, hollow, compound jets are presented in Figures 2 and 3, respectively. These figures show the jet's geometry as a function of the axial coordinate, and the leading-order axial velocity profile which increases sharply near the downstream or take-up point. Also illustrated in the figures is the axial traction on the inner jet which also exhibits a sharp increase near the downstream boundary, whereas the ratio of the axial traction in the outer liquid to that of the inner one decreases along the jet until a value equal to one is reached. This ratio increases as the capillary number and the pressure of the gases enclosed by the jet are decreased. The jet's radii increase as p_i is increased. Although not shown here, it has also been observed that ratio of traction forces increases as the Reynolds-to-Froude number ratio and μ_1/μ_2 decrease, and as ρ_1/ρ_2 , σ/σ_2 , σ_1/σ_2 , p_e , the volumetric flow rates of the inner (\dot{v}_1) and outer (\dot{v}_2) liquids and the Reynolds number increase, for steady, hollow, compound jets.

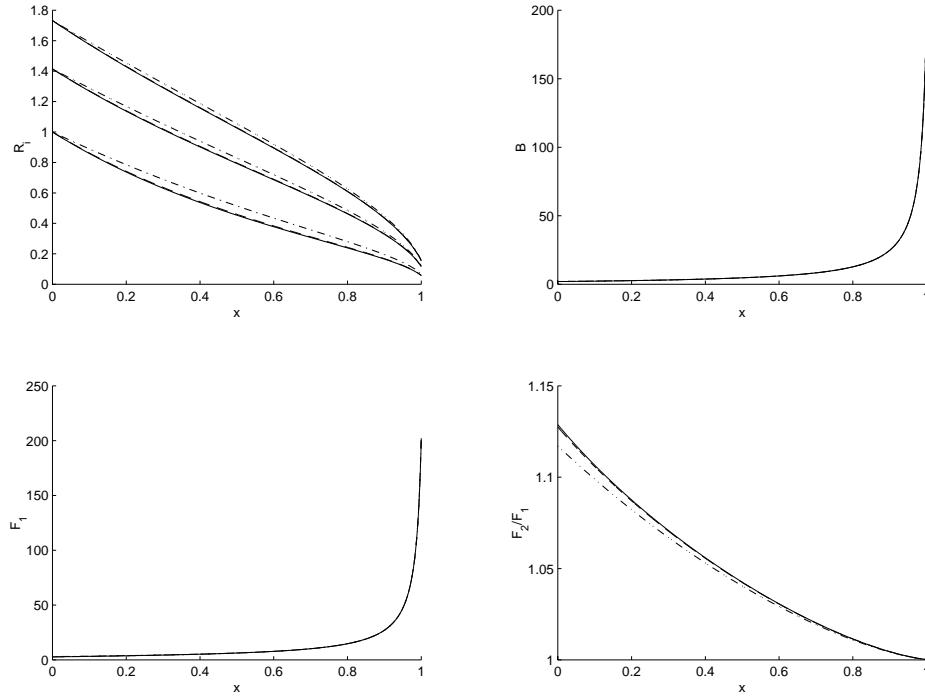


Figure 3: Hollow, compound jet's geometry (top left), axial velocity (top right), axial traction in the inner liquid (bottom left) and ratio of axial traction in the outer liquid to that in the inner one (bottom right) as function of the axial coordinate. ($Re = Re/Fr = \rho_1/\rho_2 = \mu_1/\mu_2 = \sigma/\sigma_2 = \sigma_1/\sigma_2 = \dot{v}_1 = \dot{v}_2 = Ca = 1$, $p_e = 0$; $p_i = 0$: solid lines; $p_i = 0.1$: dashed lines; $p_i = 1$: dashed-dotted lines).

The effects of time-dependent variations in the leading-order velocity at the the upstream and downstream boundaries have also been analyzed numerically for the cases in which these velocities increase or decrease linearly as functions of time and for cases in which these velocities oscillate in a sinusoidal manner. In the latter, a new nondimensional number, i.e., the Strouhal number, appears in the boundary conditions; this number represents the ratio of a residence time to the period of the imposed velocity fluctuations. These time-dependent studies were aimed at assessing the stability of hollow, compound jets and determining their nonlinear coupling with the pressure variations that occur in the gases enclosed by the jet on account of the changes in its geometry. Since the flows considered here correspond to low Reynolds numbers, the gases enclosed by the hollow, compound jet were assumed to behave polytropically.

Figures 4 and 5 show the jet's geometry and axial velocity component at the takeup point

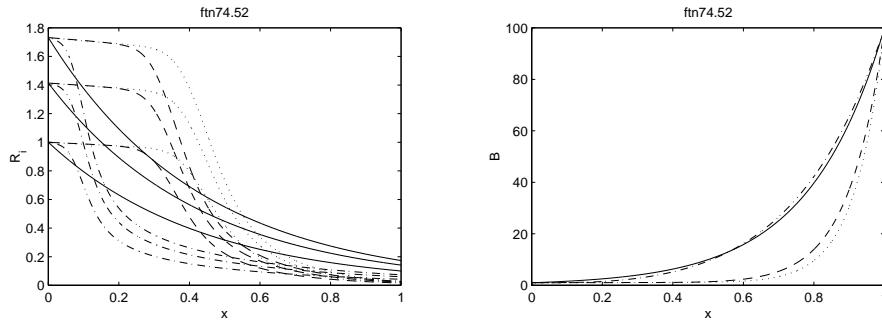


Figure 4: Hollow, compound jet's geometry (left) and axial velocity component at the takeup point (right) as function of the axial coordinate. ($Re = 10^{-4}$, $Re/Fr = 0$, $\rho_1/\rho_2 = 10$, $Ca = \infty$, $\mu_1/\mu_2 = 1$, $\sigma/\sigma_2 = \sigma_1/\sigma_2 = 0.1$, $\dot{v}_1 = \dot{v}_2 = 0.5$, $p_e = p_i = 0$, $a = 0.1$, $S = 1$; $t = 0$: solid lines; $t = 50$: dashed lines; $t = 100$: dashed-dotted lines; $t = 150$: dotted lines.

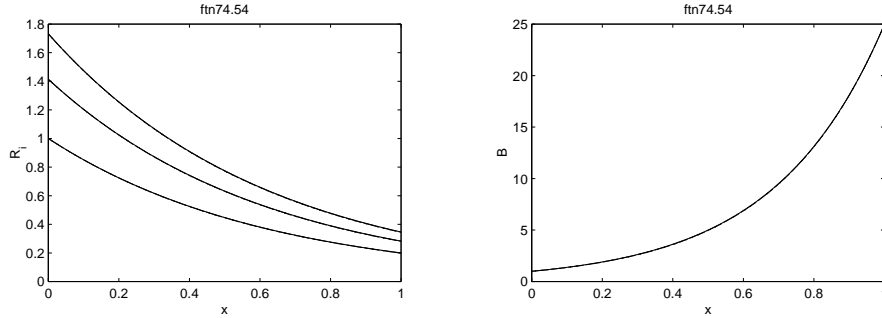


Figure 5: For caption, see Figure 4.

as function of the axial distance at four different times when $B(0, t) = 1 + a \sin(St)$ and $B(1, t) = B_s(1 + a \sin(St))$, respectively, $a = 0.1$ and $S = 1$, where S is the Strouhal number and B_s denotes the steady downstream velocity corresponding to $a = 0$, for three different values of B_s . For these parameters, the jet's geometry becomes a quasiperiodic function of time and the ratio of axial tractions oscillates in a quasiperiodic manner for $B_s = 100$, the axial traction force is more sensitive to velocity variations at the downstream boundary than to those at the upstream boundary on account of the larger axial velocity and the steep gradients at the take-up point. The results presented in Figures 4 and 5 illustrate the initial transients in the jet's geometry and show the presence of fronts.

The jet's geometry and ratio of the axial traction in the inner liquid to that in the outer one as function of the axial distance were also determined when $B(0, t) = 1 + at$ for $t \leq t_r$, $a = 0.5$ and $t_r = 1$ and the results indicate that the jet's radii increase with time until a steady state corresponding to $B(0, t) = 1.5$ is reached, whereas the ratio of traction forces first increases and then decreases until a steady state is reached. The ratio of traction forces at $t = 1$ is about 10% larger than at $t = 0$. For $a = 0.1$ and $t_r = 5$, the results indicate that the largest ratio of traction forces may be larger than 2% its initial value even though its initial and final steady values are exactly the same as the ones corresponding to $a = 0.5$ and $t_r = 1$. This large increase in the axial traction ratio as a increases while $at_r = \text{constant}$ may cause fiber rupture. Results not shown here indicate that the traction force ratio may reach large values under transient conditions which may cause fiber rupture or fiber slippage under cooling and solidification.

Acknowledgements. The research reported in this paper was supported by Project PB97-1086 from the D.G.E.S. of Spain.